*Int. J. Electrochem. Sci.*, 12 **(2017)** 3814 – 3825, doi: 10.20964/2017.05.64

International Journal of
ELECTROCHEMICAL
SCIENCE
www.electrochemsci.org

# CdSe/ZnS Quantum Dot (QD) Sensitized Solar Cell Utilizing a Multi-Walled Carbon Nanotube Photoanode on a Stainless Steel Substrate

*Junthorn Udorn*[1,*], *Shengwen Hou*[1], *Chaoyang Li*[1,2], *Akimitsu Hatta*[1,2], *Hiroshi Furuta*[1,2,*]

[1]Electronic and Photonic Systems Engineering, Kochi University of Technology, Tosayamada-cho, Kami, Kochi 782-0003, Japan
[2]Center for Nanotechnology, Research Institute, Kochi University of Technology, Tosayamada-cho, Kami, Kochi 782-0003, Japan
[*]E-mail: 178002a@gs.kochi-tech.ac.jp, furuta.hiroshi@kochi-tech.ac.jp

*Received:* 9 Decemeber 2016 / *Accepted:* 18 March 2017 / *Published:* 12 April 2017

Multi-walled carbon nanotube (MWCNT) forests grown on a stainless steel substrate were used as a photoanode in CdSe/ZnS (core/shell) quantum dot (QD) sensitized solar cells (QDSSCs). QD-treated MWCNTs on the conductive metal stainless steel substrate showed a higher power conversion efficiency (PCE) of 0.015% than those grown on a doped silicon substrate with a PCE of 0.005% under AM 1.5 sunlight intensity (100 mW/cm$^2$). This higher efficiency can be attributed to the lower sheet resistance of 0.0045 Ω/sq for the metal substrate than that for doped silicon of 259 Ω/sq. The relationship between the total reflectance of the as-prepared CNT photoanode and the PCE was investigated for CNTs of various heights and amounts of QDs. A QDSSC fabricated using a CNT photo anode with a height of 25 μm showed the highest efficiency of 0.014%, while a pristine CNT forest showed the lowest total reflectance of 1.9%, which indicates a higher surface area of CNTs and a larger amount of QDs. The as-grown 25-μm CNTs treated with QDs containing in a toluene solution of 25-μL of exhibited the highest PCE of 0.015%, due to the larger surface area of the CNTs and the higher light absorption from the large amount of QDs on the CNTs.

**Keywords:** Multi-walled carbon nanotubes (MWCNTs), Quantum dots (QDs), Quantum dot sensitized solar cells (QDSSCs), Power conversion efficiency (PCE)

## 1. INTRODUCTION

The extraordinary mechanical, chemical, and electronic properties of carbon nanotubes (CNTs) make them outstanding materials for energy applications [1–3]. A major challenge in solar cell applications is the development of modified CNT structures for use as transparent electrodes [4]. The modified CNT structure is expected to be a good material for use as a counter electrode or photo-anode

[4] with semiconducting quantum dots (QDs) in order to harvest a broader range of light from the ultraviolet (UV) to the infrared (IR) [5]. We have reported a significant increase in optical total reflectance using a structural modification of CNT honeycombs [6], which will increase the utility of CNT honeycomb structures in high-efficiency solar cells. QD-decorated CNTs exhibit efficient charge transfer from photo-excited QDs to the CNTs [7]. QD sensitized solar cells (QDSSCs) have attracted considerable interest from researchers because their power conversion efficiency (PCE) may exceed the Shockley and Queisser limits [8, 9]. In particular, QDs can harvest a broad range of optical wavelengths by multiple exciton generation (MEG), thus improving the photovoltaic efficiency [10–12]. Optical absorption by QDs fabricated from materials such as CdS [13], CdSe [14], and CdSe/ZnS [15] is intrinsically tuneable from the UV to the near-IR due to the particle-size dependence of the bandgap energy. A major advantage of QDs as light sensitizers compared with conventional dyes is that electron recombination is suppressed, thereby improving the efficiency of QDSSCs [16–18]. One-dimensional (1D) wires, of e.g., $TiO_2$ [19, 20], ZnO [21, 22], and Si [23, 24] have been extensively used for electron transfer from QDs to electrodes. In particular, CNTs have arisen as a superior candidate 1D wire electrode material for QDSSC [2, 25, 26] because of their large surface area, high conductivity, high aspect ratio, and chemical stability. Due to their excellent electrical and thermal conductivity, flexible metal substrates serving as a counter electrode of DSSCs can reduce both the sheet resistance and production cost of solar cells [27–29]. It was previously reported the PCE of QDs/Si coaxial nanowires on the gold (Au) sputtering metal electrode in QDSSCs shows 0.253% [30]. To the best of our knowledge, there are no reports of QDSSCs in which QD-treated CNT forest photoanodes are fabricated on a metal substrate.

In this study, CNT forests grown on stainless steel serving as a photoanode for CdSe/ZnS core/shell QDSSCs are investigated as a means of improving photovoltaic efficiency. The efficiency was compared for samples of QDSSCs on a metal stainless steel substrate, QDSSCs on a doped silicon substrate, and QDSSCs with a photoanode of randomly oriented CNT (buckypaper) films on a metal stainless steel substrate. The relationship between the optical total reflectance of as-grown CNTs and the PCE, and the impact of the CNT height and QD quantity on the PCE were investigated.

## 2. MATERIAL AND METHODS

Vertically aligned multi-walled carbon nanotube (MWCNT) forests with tube diameters of 30–65 nm and heights of ~15 μm were prepared by a catalytic thermal chemical vapour deposition (CVD) method with an annealing time of 2.5 min in a hydrogen flow of 65 sccm at 28 Pa and 730°C, followed by CNT synthesis at 730°C with a carbon source gas of acetylene ($C_2H_2$) gas at 54 Pa for 10 min on Fe/Al (5/50 nm in thickness) bi-layered catalyst films on a sheet of stainless steel SUS304 (68% iron, 19% chromium, 10% manganese, 1% silicon, and 2% other compounds). The Fe/Al catalyst films on the stainless steel sheet were deposited by magnetron sputtering under an argon flow of 10 sccm, a pressure of 0.8 Pa, and a discharge current of 40 mA for 21 min for Al and 2.5 min for Fe. CNT buckypaper films were prepared by dipping vertically aligned CNTs grown on the stainless steel sheet into a methanol solution for 5 min, and then drying them in air at room temperature. The morphologies and heights of the as-grown CNT forests and modified CNT structures were characterized using field-

emission scanning electron microscopy (FE-SEM; JEOL JSM-5310). The total reflectance in the UV–vis region was measured using a spectrophotometer (HITACHI U-3900). The photoluminescence spectra were measured using an iHR320 Micro-PL/Raman spectroscope (Horiba) with a 325-nm wavelength He-Cd laser source with a power of 1 mW. Solar cells were fabricated from as-grown CNT forests and CNT buckypaper films as photoanodes, treated with CdSe/ZnS (core/shell) quantum dots in toluene solutions as a sensitizer with a particle size of 3.4 nm (Lumidot$^{TM}$, Aldrich). Indium tin oxide (ITO) glass with a sheet resistance of ~15 Ω/sq was used as a counter electrode, and the 0.1-cm$^2$ active area between the two electrodes was filled with an iodide electrolyte solution ($I^-/I_3^-$). The J–V characteristics of the cells were recorded with a computer-controlled digital source meter (Keithley Model 2400) by applying an external potential bias to the cell under AM 1.5 sunlight intensity (100 mW/cm$^2$). All measurement was carried out at room temperature.

## 3. RESULTS AND DISCUSSION

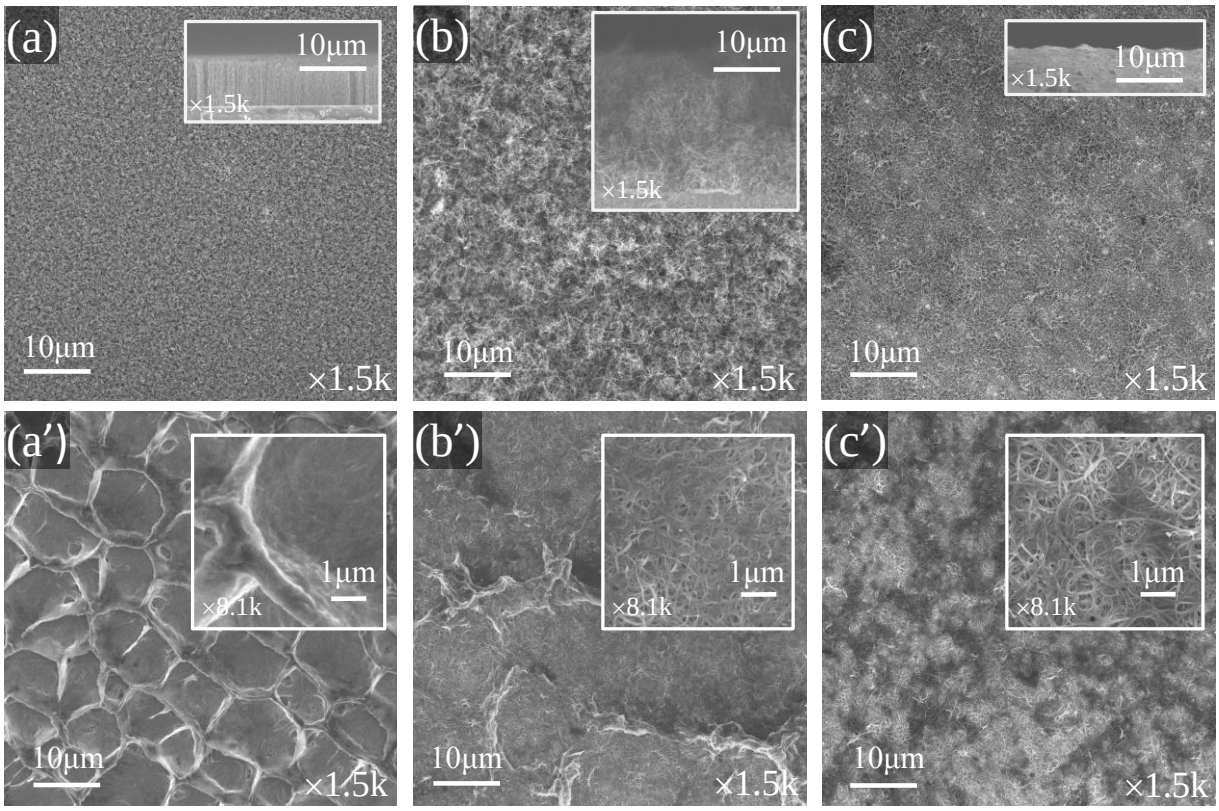


**Figure 1.** Top-view FE-SEM images of (a) as-grown CNTs on silicon substrate, (b) as-grown CNTs on stainless steel substrate, and (c) CNT buckypaper films on stainless steel substrate. The insets show cross-sectional images. CdSe/ZnS QDs-treated on (a') as-grown CNTs on silicon substrate, (b') as-grown CNTs on stainless steel substrate, (c') CNT buckypaper films on stainless steel substrate. The insets show high-magnification images. White and black bars stand for 10 and 1 μm, respectively.

Figures 1(a – c) show top-view SEM micrographs of as-grown CNTs on a silicon substrate, a stainless steel substrate, and CNT buckypaper films on a stainless steel substrate, respectively. The

insets show cross-sectional SEM images of each sample. In Fig. 1(b), the as-grown CNTs on the stainless steel have a variable height from 10 to 25 μm, whereas the as-grown CNTs on the silicon substrate in Fig. 1(a) have a higher density and a uniform height. The CNT buckypaper films have highly packed CNTs, as shown in the inset of Fig. 1(c). Figures 1(a'–c') show SEM images soaking for 1.5 min in 20 μL of QDs in toluene solutions for samples of CNT forests on Si, stainless steel, and buckypaper on stainless steel, respectively. After QD treatment, highly-packed CNT films were formed on the stainless steel, as shown in the inset of Fig. 1(b'), whereas a honeycomb-like CNT structure was formed on the silicon substrate, as shown in Fig. 1(a').

**Table 1.** Properties of QD-treated CNTs on a silicon substrate, and CNT buckypaper films on the stainless steel substrate, and QDs-treated CNTs on the stainless steel with various heights. [31]

| **Sample** | **Sheet resistance (Ω/sq)** | **Series resistance (Ω)** | **Total reflectance at 560 nm (without QDs)** | $J_{SC}$ **(mA/cm$^2$)** | $V_{OC}$ **(V)** | ***FF*** | $\eta$ **(PCE)** |
|---|---|---|---|---|---|---|---|
| QD-treated CNTs on silicon substrate | 259 | 33K | 0.98% | 0.067 | 0.21 | 38.6% | 0.005% |
| QD-treated CNT buckypaper films on SUS | 0.0046 | 14K | 4.3% | 0.068 | 0.32 | 42.9% | 0.009% |
| QD-treated 17-μm CNTs on SUS | 0.0047 | 13K | 4.1% | 0.050 | 0.38 | 56.7% | 0.011% |
| QD-treated 25-μm CNTs on SUS | 0.0045 | 13K | 1.9% | 0.057 | 0.45 | 52.2% | 0.014% |
| QD-treated 33-μm CNTs on SUS | 0.0043 | 14K | 2.2% | 0.049 | 0.40 | 65.6% | 0.013% |
| QD-treated 41-μm CNTs on SUS | 0.0043 | 13K | 2.2% | 0.056 | 0.39 | 54.4% | 0.012% |

Table 1 shows the sheet resistance, series resistance, optical total reflectance, and PCE for these samples [31]. As-grown CNTs with a height of 25 μm on a stainless steel substrate with a sheet resistance of 0.0045 Ω/sq and an optical total reflectance of 1.9% at 560 nm exhibit the highest PCE of 0.014%. Meanwhile, as-grown CNTs on a silicon substrate with a higher sheet resistance of 259 Ω/sq exhibit a PCE of 0.005%. The 2.8 times higher PCE for the former sample can be attributed to the higher conductance of the substrate. The PCE for QD-treated CNTs on the stainless steel substrate is 1.6 times higher than that for CNT buckypaper films on the same metal stainless steel substrate, which can be attributed to the higher number of QDs adsorbed on the surface of the CNTs. QD-treated CNTs on the stainless steel substrate had heights of 17, 25, 33 and 41 μm, and the PCE was the highest, at 0.014%, for a height of 25 μm. For the taller CNTs, the lower PCE could be explained by the fact that

the electron transport path was longer than the electron diffusion length, leading to increased recombination of electrons and holes [32], and hence a lower efficiency.

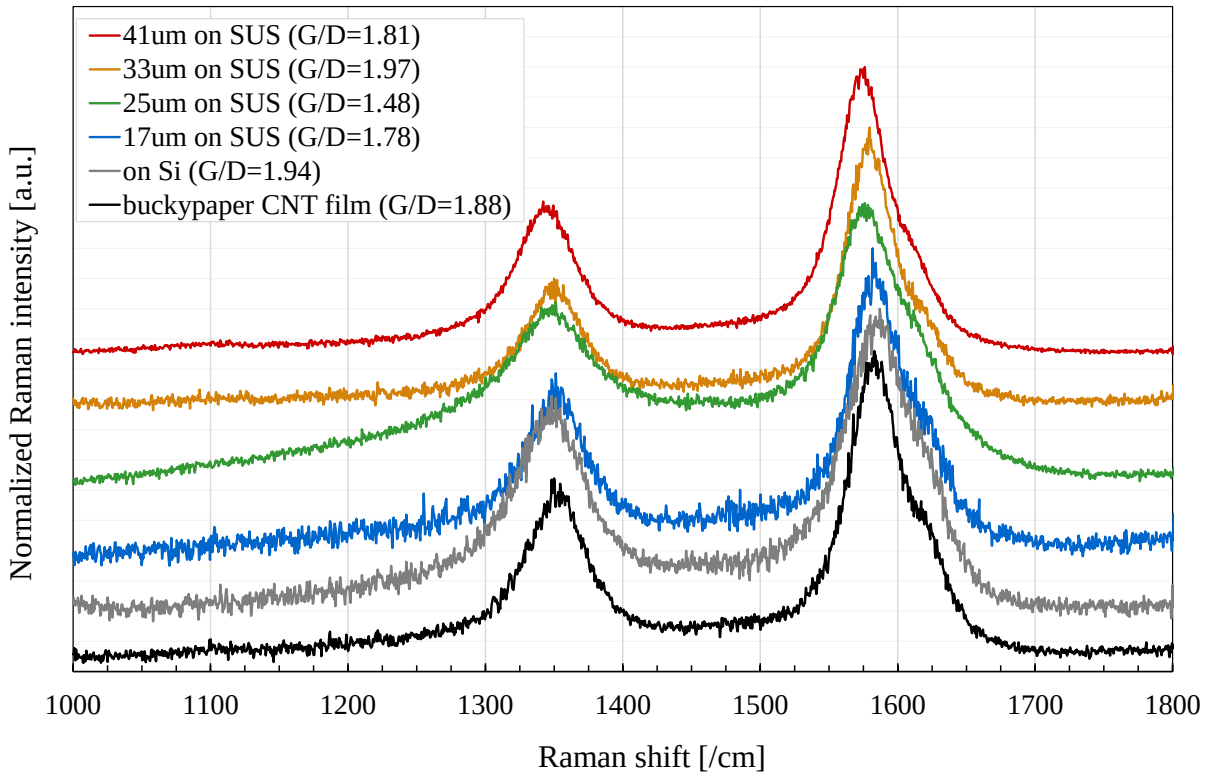


**Figure 2.** Raman spectra of as-grown CNTs on silicon substrate, CNT buckypaper films on stainless steel substrate, and as-grown CNTs with various heights on stainless steel substrate. The Raman laser wavelength was 532.8 nm.

Figure 2 shows Raman spectra of as-grown CNTs on a silicon substrate, a CNT buckypaper film, and as-grown CNTs of various heights on the stainless steel substrate. The Raman spectra of all the samples show characteristic D- and G-bands at around 1350 and 1580 $cm^{-1}$, respectively. The G/D intensity ratio indicates the amount of disorder of the CNTs and graphite crystal [33]. The G/D ratio for as-grown CNTs is 1.48–1.97, and for CNT buckypaper films on a stainless steel substrate is 1.88, which is lower than the value of 1.94 for as-grown CNTs on a silicon substrate. The G/D ratios for as-grown CNTs with heights of 33 and 41 μm are 1.97 and 1.81, respectively, indicating that a higher number of layers exist in the thicker MWCNT samples on the metal substrates compared with the thinner 17-and 25-μm height CNTs.

Figure 3 shows a schematic energy-level diagram for CNTs and CdSe/ZnS core/shell quantum dots on a metal substrate (modified from [30, 34, 35]). The excitonic transition of CdSe/ZnS corresponds to the size of the QDs of 3.4 nm and the bandgap is 2.21 eV for the wavelength of 561 nm. Excitons of electron–hole pairs are generated by absorption of light in the CdSe core. An electron generated in the conduction band of the CdSe core transfers to the CNT and is collected on the

conductive photoanode. Multi-electron generation (MEG) is also possible, generating two or more electron–hole pairs if the photon energy is greater than or equal to $2E_g$ ($E_g$: bandgap energy) for CdSe/ZnS (4.42 eV) at 280 nm in the UV region [36].

Figure 4(a) shows the total reflectance of as-grown CNTs on a silicon substrate, a CNT buckypaper film on a stainless steel substrate, and as-grown CNTs of various heights on a stainless steel substrate. For as-grown CNTs on the stainless steel before QD treatment, the strong reflection at wavelengths shorter than 380 nm can be assigned to Rayleigh scattering, which provides a higher reflectance at shorter wavelength [37]. The bandgap of CdSe ($E_g$ = 2.21 eV) corresponds to 561 nm, which is expected to be the absorption edge for QDs. The CNT buckypaper films (black line) exhibit a higher total reflectance of more than 5% at 200–561 nm due to the highly packed CNTs serving as glassy carbon to reflect light strongly [38]. As-grown CNTs on a silicon substrate (grey line) exhibit the lowest total reflectance of less than 2%, which can be attributed to the higher density of CNT forests [39]. The CNT forest with a height of 25 μm has a lower averaged total reflectance of 2.9% at a wavelength of 200 – 560 nm. This can be explained that multiple scattering of the incident light into the bottom of the CNT forest, so-called blackbody absorption [39] causes the lower total reflectance.

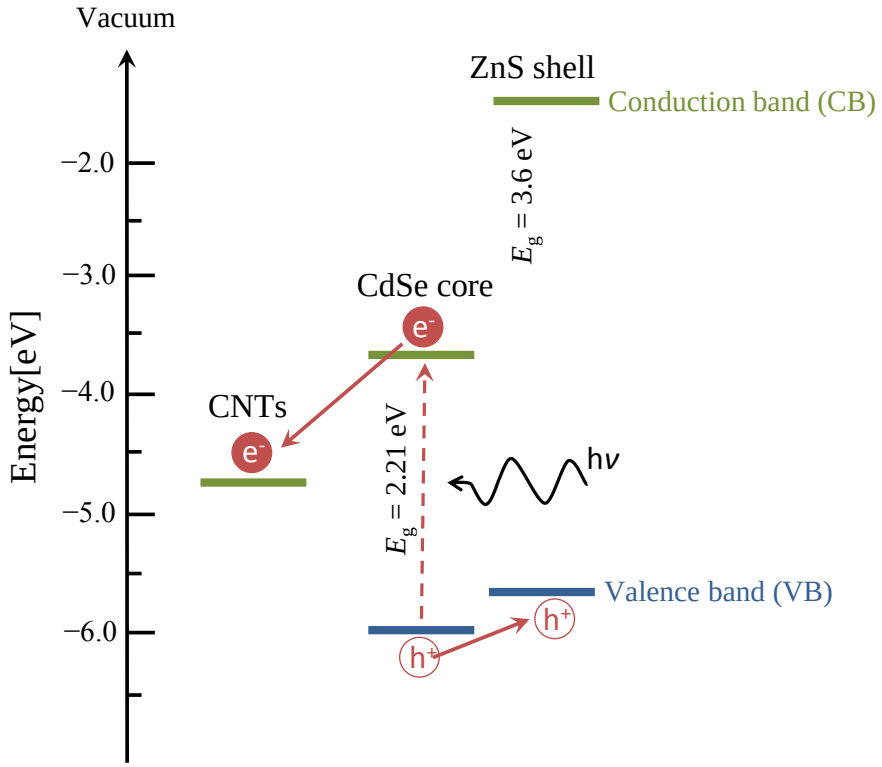


**Figure 3.** Structure schematic and energy band diagram of CdSe/ZnS (core/shell) QD-treated CNTs on a metal substrate as a photoanode.

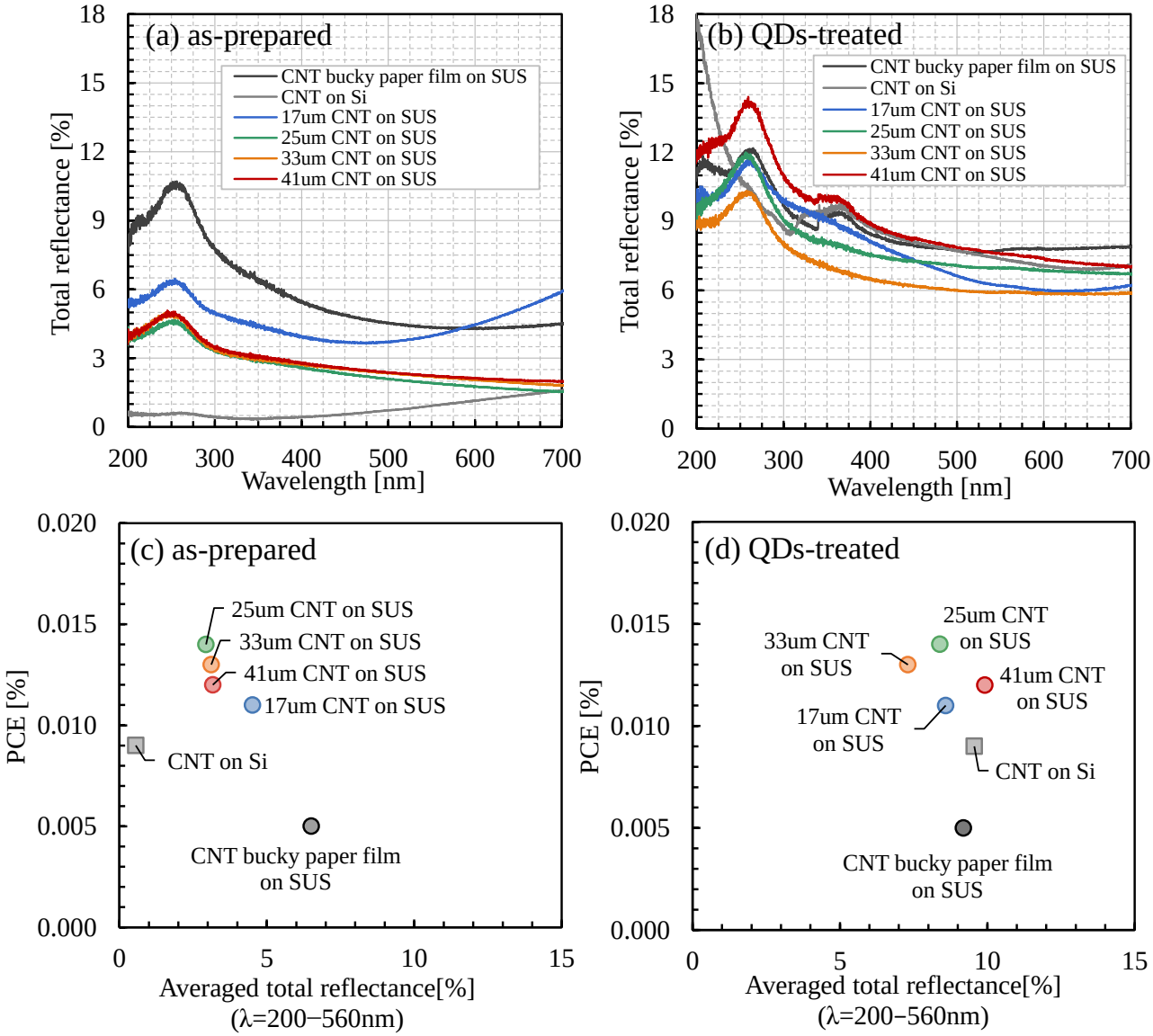


**Figure 4.** Optical total reflectance of (a) as-prepared and (b) QDs-treated CNTs on silicon substrate (grey), CNT buckypaper films on stainless steel substrate (black), and as-prepared CNTs with various heights on stainless steel substrate. PCE vs. optical total reflectance of (c) as-prepared and (d) QDs-treated CNTs.

Additionally and theoretically , the light incidence on a top surface of CNT forests with a small angle to the CNT axis in which electrons on the CNT body cannot couple with electric fields providing a low optical interaction between the CNT forests and normally incident, resulting the low total reflectance [40]. Figure 4(c) shows the relationship between the total reflectance and the PCE, which indicates that the lower total reflectance of the as-grown CNTs on the stainless steel gives a higher solar cell efficiency after QDSSC fabrication. Significantly, the PCE for QDSSCs with CNTs with heights of 25 μm on a stainless steel substrate, with the averaged total reflectance of 2.9% (green symbols), has a maximum value of 0.014%. Also, as can be seen in Fig. 4(d), the 25-μm and 33-μm height films exhibit a lower total reflectance and a higher PCE. The low total reflectance of CNT forests due to efficient absorption of light in CNTs, by the mechanism of the repeated reflection of

incident light into the CNT bottom region [39] indicates a higher CNT surface area, which is expected to adsorb a larger number of QDs to generate and transfer electrons into CNTs for the efficient photoconversion resulting in a higher PCE [41].

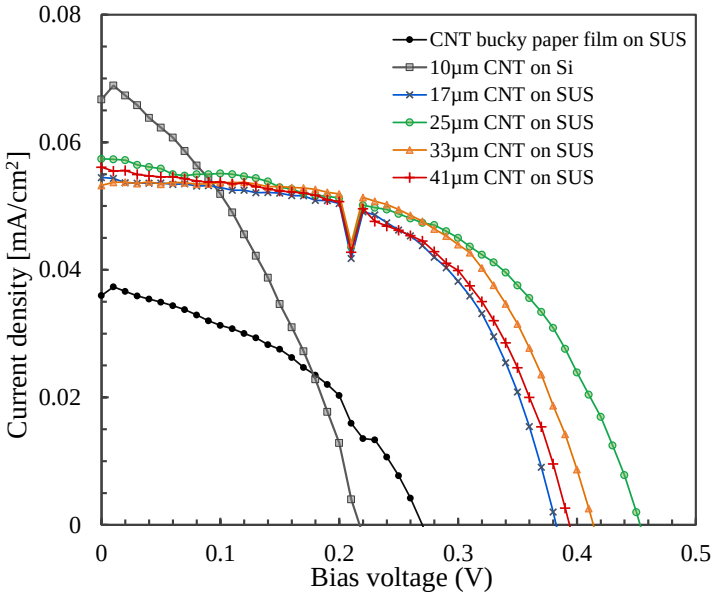


**Figure 5.** J–V curves of photovoltaic QDSSCs cells of QD-treated CNTs on silicon substrate, CNT buckypaper films on stainless steel substrate, and QDs-treated CNTs with various heights on stainless steel substrate.

Figure 5 presents J–V curves for QDSSC cells of QD-treated CNTs on a silicon substrate, QD-treated CNT buckypaper films on a stainless steel substrate, and QD-treated CNTs with various heights on a stainless steel substrate. The PCE ($\eta$) was calculated using the equation $\eta = (FF \times J_{SC} \times V_{OC}) / P_{input}$, where $FF$ is the fill factor and $P_{input}$ is the power density of the incident light. It can be seen that QD-treated CNTs with a height of 25-μm exhibit significantly better photovoltaic performance in terms of the current density ($J_{SC}$) and the open-circuit voltage ($V_{OC}$). Compared to those on the low-conductivity silicon substrate, as-grown CNTs after QD treatment on the stainless steel substrate also exhibit an improved open-circuit voltage of 0.21 to 0.45 volts (see Table 1). This is evidence that the low resistivity of the conductive substrate, which shows excellent electrical and thermal conductance to enhance electron transport and inhibit electron recombination [27, 28], gives an increased open-circuit voltage, leading to improved solar cell efficiency. The QD-treated CNTs with heights of 25 μm exhibit a higher $V_{OC}$ of 0.45 volts and also slightly improves the $V_{OC}$ from 0.32 to 0.45 volts as compared with CNT buckypaper films. In addition, the energy barrier at the QDSSC/CNT interface can suppress interfacial recombination [28,42], leading to an increased $V_{OC}$, which is expected for CNT forests directly grown on metal substrates. The increase in the PCE is an indication of improved charge collection and transport due to introducing the CNTs forest directly grown on the metal substrate at a significant specific height as an electrode scaffold in the photoanode of solar cells.

The amount of QDs in toluene solutions was varied to examine the influence on the PCE. Figure 6(a) shows the photoluminescence (PL) intensities for as-grown CNTs with heights of 25 μm on a stainless steel substrate for varied amounts of QD solutions. As shown in Fig. 6(a), clear PL peaks for QD-treated CNT forests are found at 570 nm, which corresponds to the bandgap ($E_g$) of 2.21 eV (561 nm). Comparing the different amount of QDs, it is seen that the highest peak intensity is for 15 μL of QDs, and the largest amount of QDs at 25 μL yields the second highest peak intensity. A variation of the PL peak intensity due to the thickness distribution was observed, shown in the inset of Fig. 6(a) as error bars. The inset of Fig. 6(a) shows the dependence of the PL peak intensity at 570 nm on the volume of the QD solution. In particular, the PCE for a CNT photoanode with 25-μL QD treatment and 7.2% total reflectance has a maximum value of 0.015% (see Table 2). This confirms that a lower total reflectance (higher absorption) contributes to efficient absorption by QDs to increase charge collection for the photoanode leading to improved solar cell efficiencies.

**Table 2.** Properties of as-grown CNTs after QD solution treatment on the stainless steel substrate for varied amounts of QDs

| | **Total reflectance at 560 nm (with QDs)** | $J_{SC}$ **(mA/cm$^2$)** | $V_{OC}$ **(V)** | ***FF*** | $\eta$ **(PCE)** |
|---|---|---|---|---|---|
| As-grown CNTs with 10-μL QDs | 6.8% | 0.058 | 0.36 | 51.8% | 0.011% |
| As-grown CNTs with 15-μL QDs | 8.9% | 0.055 | 0.29 | 54.2% | 0.008% |
| As-grown CNTs with 20-μL QDs | 7.8% | 0.061 | 0.31 | 52.1% | 0.010% |
| As-grown CNTs with 25-μL QDs | 7.2% | 0.058 | 0.62 | 41.6% | 0.015% |

This confirms that a lower total reflectance (higher absorption) contributes to efficient absorption by QDs leading to improved solar cell efficiencies. A variation of the PL peak intensity due to the thickness distribution was observed, shown in the inset of Fig. 6(a) as error bars. Than inset of Fig. 6(a) shows the dependence of the PL peak intensity at 570 nm on the volume of the QD solution.

Figure 7 presents *J–V* curves for as-grown CNTs on a stainless steel substrate with various amounts of QDs. The as-grown CNTs treated with 25 μL of QDs also exhibit an improvement in the open-circuit voltage from 0.36 to 0.62 V compared with 10 μL of QDs (see Table 2). The data shows that the efficiency of as-grown CNTs with 25 μL of QDs is the highest at 0.015%. Thus, larger amounts of QDs lead to improved solar cell efficiency because they can absorb direct incident light and reflected light from CNTs to generate more electron–hole pairs for photoanodes to improve the solar cell efficiency.

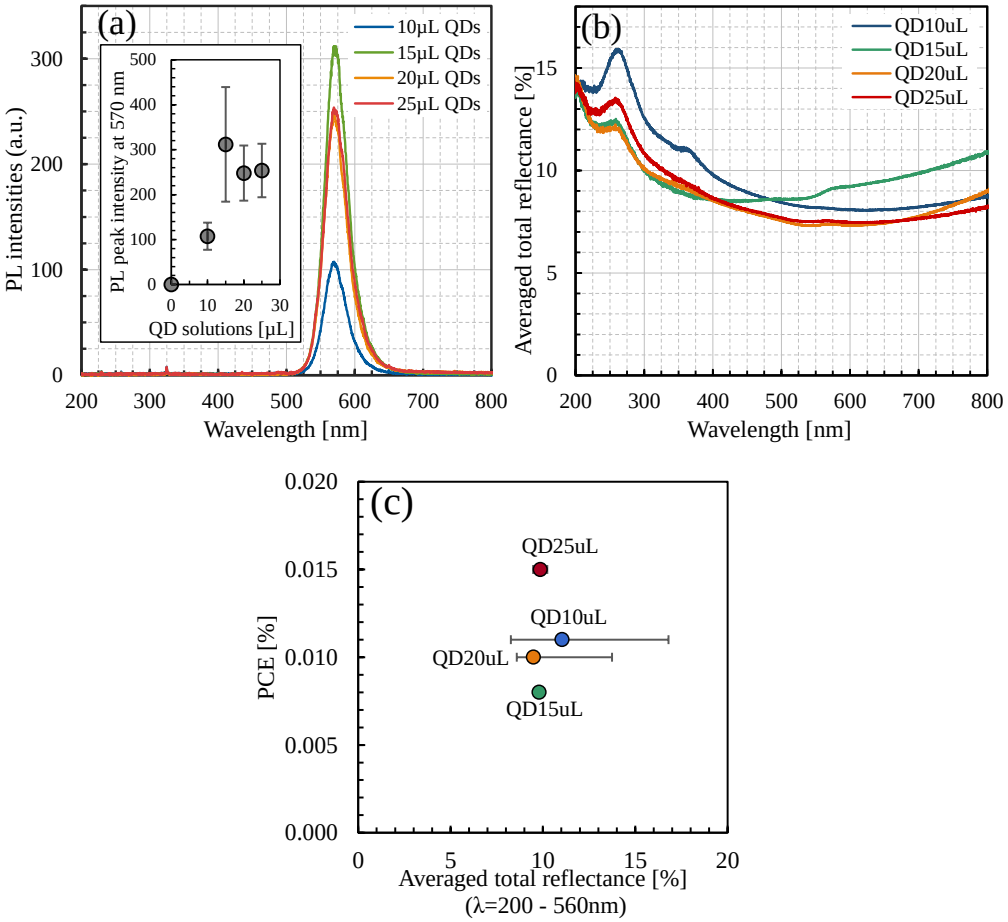


**Figure 6.** (a) Photoluminescence (PL) spectra of as-grown 25-μm-height CNTs on stainless steel substrate for different amounts of CdSe/ZnS (core/shell) quantum dots of 10, 15, 20, and 25 μL. The excited laser wavelength was 351 nm. Inset: PL peak intensities vs. QD solution volume. (b) Total reflectance for various QDs solutions. (c) PCE vs. average total reflectance for 200–560 nm.

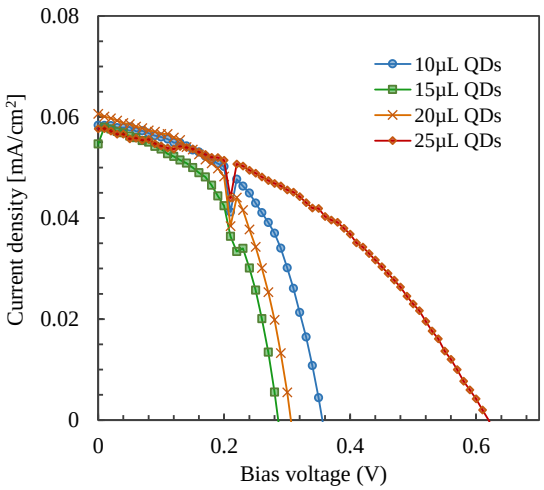


**Figure 7.** *J–V* curves of as-grown CNTs on stainless steel substrates for various amounts of QD solutions.

## 4. SUMMARY

This paper reports the first QDSSCs with photoanodes of MWCNTs on a metal substrate. It was found that the PCE for such QDSSCs on stainless steel substrates was three times higher than those on a low-resistivity (0.15 Ω·cm), doped silicon substrate. A QD-treated MWCNT forest on a metal substrate was found to had a resistance of 0.0045 Ω/sq and exhibited a higher PCE of 0.015%, whereas QD-treated MWCNTs on a doped silicon substrate had a resistance of 259 Ω/sq and a lower efficiency of 0.005%. This difference could be attributed to the fact that the very low sheet resistivity of a metal substrate gives a higher electrical conductance leading to a higher cell efficiency. The relationship between the total reflectance of QD-treated CNT forests and the PCE was investigated. It was shown that the lower total reflectance QD-treated CNT forest of 25-μm height achieved a higher PCE of 0.014%, likely due to the higher light absorption in the QDs. The as-grown 25-μm CNTs combined with 25 μL of QDs in toluene solutions exhibited the highest PCE of 0.015%, due to the larger surface area of the CNTs and the higher light absorption from the large amount of QDs on the CNTs Although the efficiency is currently low compared with that of high-performance DSSCs or QDSSCs, the successful incorporation of QDs with a CNT forest on a conductive substrate as a photoanode for solar cells has been demonstrated for the first time.

ACKNOWLEDGEMENTS
This work was supported by JSPS KAKENHI Grant (No. 24560050) and by a grant from the Japanese Government (MEXT) Scholarship (No. 132308). The author would like to thank Mr. Sachio Hayashi for his support in the experiments.

## References

1. S. Iijima, *Nature* 354 (1991) 56.
2. P. Dong, C.L. Pint, M. Hainey, F. Mirri, Y. Zhan, J. Zhang, M. Pasquali, R. H. Hauge, R. Verduzco, M. Jiang, H. Lin, J. Lou, *ACS Appl. Mater. Interfaces* 3 (2011) 3157.
3. H. W. Zhu, H. F. Zeng, V. Subramanian, C. Masarapu, K. H. Hung, B. Q. Wei, *Nanotechnology.* 19 (2008) 5.
4. K. Cui, T. Chiba, S. Omiya, T. Thurakitseree, P. Zhao, S. Fujii, H. Kataura, E. Einarsson, S. Chiashi, S. Maruyama, *J. Phys. Chem. Lett*. 4 (2013) 257.
5. S. Hickey, D. Riley, E. Tull, *J. Phys. Chem*. B 104 (2000) 7623.
6. J. Udorn, A. Hatta, H. Furuta, *Nanomaterials* 6 (2016) 202.
7. J. M. Haremza, M. A. Hahn, T. D. Krauss, S. Chen, J. Calcines, *Nano Lett*. 2 (2002) 1253.
8. K. Watanabe, R. Tsuchiya, K. Oda, J. Yamamoto, T. Hattori, M. Matsumura, M. Kudo, K. Torii, *Int. Electron Devices Meet., IEEE*, (2011) 36.4.1.
9. O. D. Miller, E. Yablonovitch, S. R. Kurtz, *IEEE J. Photovoltaics* 2 (2012) 303.
10. P. Péchy, T. Renouard, S. M. Zakeeruddin, R. Humphry-Baker, P. Comte, P. Liska, L. Cevey, E. Costa, V. Shklover, L. Spiccia, G. B. Deacon, C. A. Bignozzi, M. Grätzel, *J. Am. Chem. Soc*. 123 (2001) 1613.
11. A. V. Barve, S. Meesala, S. Sengupta, J.-O. Kim, S. Chakrabarti, S. Krishna, *Appl. Phys. Lett*. 100 (2012) 191107.
12. J. D. Mar, X. L. Xu, J. J. Baumberg, A. C. Irvine, C. Stanley, D. A. Williams, *J. Appl. Phys*. 110 (2011) 053110.

13. K. Yu, G. Lu, K. Chen, S. Mao, H. Kim, J. Chen, *Nanoscale*. 4 (2012) 742.
14. J. Tian, Q. Zhang, L. Zhang, R. Gao, L. Shen, S. Zhang, X. Qu, G. Cao, *Nanoscale* 5 (2013) 936.
15. S.-W. Baek, J.-H. Shim, H.-M. Seung, G.-S. Lee, H.-J. Pyo, K.-S. Lee, J.-G. Park, *Nanoscale*. 6 (2014) 12524.
16. E. T. Hoke, I. T. Sachs-Quintana, M. T. Lloyd, I. Kauvar, W. R. Mateker, A. M. Nardes, C. H. Peters, N. Kopidakis, M. D. McGehee, *Adv. Energy Mater*. 2 (2012) 1351.
17. Y. Li, L. Wei, R. Zhang, Y. Chen, J. Jiao, *J. Nanomaterials*. 2012 (2012) 1.
18. M. C. Beard, *J. Phys. Chem. Lett*. 2 (2011) 1282.
19. I. Zarazúa, E. De La Rosa, T. López-Luke, J. Reyes-Gomez, S. Ruiz, C. Ángeles Chavez, J.Z. Zhang, *J. Phys. Chem*. *C* 115 (2011) 23209.
20. N. Guijarro, T. Lana-Villarreal, I. Mora-Sero, J. Bisquert, R. Gomez, *J. Phys. Chem*. C 113 (2009) 4208.
21. C. Li, J. Xia, Q. Wang, J. Chen, C. Li, W. Lei, X. Zhang, *ACS Appl. Mater. Interfaces* 5 (2013) 7400.
22. Y. Zhang, T. Xie, T. Jiang, X. Wei, S. Pang, X. Wang, D. Wang, *Nanotechnology* 20 (2009) 155707.
23. T. Takahashi, *Jpn. J. Appl. Phys*. 50 (2011) 4208.
24. R. Jeyakumar, T. K. Maiti, A. Verma, *Sol. Energy Mater. Sol. Cells* 109 (2013) 199.
25. F. Malara, M. Manca, L. De Marco, P. Pareo, G. Gigli, *ACS Appl. Mater. Interfaces* 3 (2011) 3625.
26. T. Peng, P. Zeng, D. Ke, X. Liu, X. Zhang, *Energy & Fuels* 25 (2011) 2203.
27. M. G. Kang, N.-G. Park, K. S. Ryu, S. H. Chang, K.-J. Kim, *Sol. Energy Mater. Sol. Cells* 90 (2006) 574.
28. K. Miettunen, J. Halme, M. Toivola, P. Lund, *J. Phys. Chem.* C 112 (2008) 4011.
29. T. L. Ma, X. M. Fang, M. Akiyama, K. Inoue, H. Noma, E. Abe, *J. Electroanal. Chem*. 574 (2004) 77.
30. Y. Hsieh, M. Lee, G. Wang, *Int. J. Photoenergy*. 2015 (2015) 1.
31. J. Udorn, H. Sachio, S. Hou, C. Li, A. Hatta, H. Furuta, CdSe / ZnS (Core / Shell ) Quantum Dots Multi-Wallled Carbon Nanotubes ( MWCNTs ) on a Stainless Steel as a Photoanode in Solar Cells, *Proceedings of PHOTOPTICS 2017*, (PORTO, Portugal, Feb. 2017) (to be published).
32. J. Wei, C. Zhang, Z. Du, H. Li, W. Zou, *J. Mater. Chem. C* (2014) 4177.
33. P. Tan, S.-L. Zhang, K. T. Yue, F. Huang, Z. Shi, X. Zhou, Z. Gu, *J. Raman Spectrosc.* 28 (1997) 369.
34. L.-H. Lai, W. Gomulya, L. Protesescu, M. V. Kovalenko, M.A. Loi, *Phys. Chem. Chem. Phys.* 16 (2014) 7531.
35. H.-Y. Si, C.-H. Liu, H. Xu, T.-M. Wang, H.-L. Zhang, Nanoscale Res. Lett. 4 (2009) 1146.
36. P. V Kamat, *J. Phys. Chem. C* 112 (2008) 18737.
37. Z. Yu, and Louis Brus, *J. Phys. Chem. B* 105 (2001) 1123.
38. A. A. Shabaneh, S.H. Girei, P.T. Arasu, S.A. Rashid, Z. Yunusa, M.A. Mahdi, S. Paiman, M.Z. Ahmad, M.H. Yaacob, *IEEE Photonics J.* 6 (2014) 6802910.
39. K. Mizuno, J. Ishii, H. Kishida, Y. Hayamizu, S. Yasuda, D.N. Futaba, M. Yumura, K. Hata, *Proc. Natl. Acad. Sci. USA* 106 (2009) 6044.
40. Y. Murakami, E. Einarsson, T. Edamura, S. Maruyama, *Phys. Rev. Lett.* 94 (2005) 1.
41. I. Robel, B. A. Bunker, P. V. Kamat, *Adv. Mater.* 17 (2005) 2458.
42. C.V.V.M. Gopi, M. Venkata-Haritha, S.-K. Kim, H.-J. Kim, *Nanoscale* 7 (2015) 12552.